DOI: 10.1002/anie.201309307

Nanoscale Critical Phenomena

Identification of a Critical Intermediate in Galvanic Exchange Reactions by Single-Nanoparticle-Resolved Kinetics**

*Jeremy G. Smith, Qing Yang, and Prashant K. Jain**

Abstract: *The realization of common materials transformations in nanocrystalline systems is fostering the development of novel nanostructures and allowing a deep look into the atomistic mechanisms involved. Galvanic corrosion is one such transformation. We studied galvanic replacement within individual metal nanoparticles by using a combination of plasmonic spectroscopy and scanning transmission electron microscopy. Single-nanoparticle reaction trajectories showed that a Ag nanoparticle exposed to Au^{3+} makes an abrupt transition into a nanocage structure. The transition is limited by a critical structural event, which we identified by electron microscopy to comprise the formation of a nanosized void. Trajectories also revealed a surprisingly strong nonlinearity of the reaction kinetics, which we explain by a model involving the critical coalescence of vacancies into a growing void. The critical void size for galvanic exchange to spontaneously proceed was found to be 20 atomic vacancies.*

Critical phenomena are central to solid-state transformations. Some well-known examples include the development of photographic films through the formation of latent Ag_4 clusters,[1] spinodal decomposition in alloys,[2] and biomineralization.[3] These phenomena are characterized by an energetically uphill step, often involving the formation of critical-sized nuclei, following which the transformation proceeds spontaneously. A wealth of physical insight into materials transformations can be obtained by capturing the nucleation dynamics. However, such dynamics occur within nanosized grains or domains; therefore, methods for single-nanodomain resolution[4–7] are required to capture them. In bulk-scale measurements, useful dynamics are smeared out owing to ensemble averaging over a large number of nanosized domains that are not in temporal phase with one another. In this study, we employed plasmonic spectroscopy to probe with single-nanoparticle resolution the dynamics of a common solid-state transformation and identified a critical structural event in the transformation.

We studied the dynamics of a galvanic replacement reaction: an electrochemical process driven by a difference in redox potentials of two metallic species.[8,9] The more reactive metal undergoes oxidative dissolution concomitant to the deposition of a less reactive metal from its ionic solution. Galvanic reactions are central to the understanding and control of metal corrosion,[10] the formation of protective coatings,[11] and the fabrication of nanostructured and porous metal structures.[12] Galvanic replacement is also becoming a facile method for the production of hollow nanostructures of a variety of metals,[13,14] semiconductors,[15] and metal oxides,[16] which are finding application in medicine,[17] catalysis,[18] and sensing.[19]

We chose as a model system the galvanic replacement of Ag nanospheres with Au^{3+}. The Ag nanospheres serve as a sacrificial template for the formation of hollow Au nanostructures with a high level of porosity.[20] Both Au and Ag nanostructures are plasmonic materials, with strong resonant scattering in the visible region, thus making these nanostructures amenable to optical probing at the single-particle level.[21–25] We used the well-established method of dark-field scattering spectroscopy to monitor in real time, in solution, individual Ag nanoparticles undergoing a galvanic transformation into Au-based nanostructures. Ag nanoparticles (40 nm diameter polycrystalline spheres from Ted Pella) were deposited sparsely on the base of a home-built glass microfluidic cell (see the Supporting Information). Sparse distribution of the nanoparticles ensures that the average separation between individual nanoparticles is greater than the diffraction limit, thus enabling the resolution of individual nanoparticles.

Figure 1 shows dark-field scattering snapshots of nanoparticles at various points during a galvanic replacement reaction (see also Movies 1–3 in the Supporting Information). The brightly scattering Ag nanoparticles (top frame) transition one nanoparticle at a time to dimly scattering Au/Ag nanocages (bottom frame). These transitions are characterized by a red shift of the surface plasmon resonance spectrum, with a corresponding decrease in scattering intensity

[*] J. G. Smith, Q. Yang,[+] Prof. P. K. Jain
Department of Chemistry
University of Illinois at Urbana Champaign
600 South Mathews Avenue, Urbana, IL 61801 (USA)
E-mail: jain@illinois.edu
Homepage: http://www.nanogold.org
Prof. P. K. Jain
Department of Physics and Materials Research Laboratory
University of Illinois at Urbana
Champaign, Urbana, IL 61801 (USA)
[+] Present address:
Department of Chemistry, University of California at Los Angeles
Los Angeles, CA 90095 (USA)

[**] J.G.S and P.K.J. designed the experiments. J.G.S. performed the experiments. Q.Y. performed preliminary studies. P.K.J. conceived the project and developed the theory. J.G.S. and P.K.J. wrote the manuscript. We thank M. J. Russell for preliminary studies. J.G.S. was partially supported by a James R. Beck Fellowship and the National Science Foundation through the NanoBIO Node to the Network for Computational Nanotechnology (NCN; Cooperative Agreement No. EEC 12-27034). The research was carried out in part at the Frederick Seitz Materials Research Laboratory Central Facilities, University of Illinois.

Supporting information for this article is available on the WWW under http://dx.doi.org/10.1002/anie.201309307.

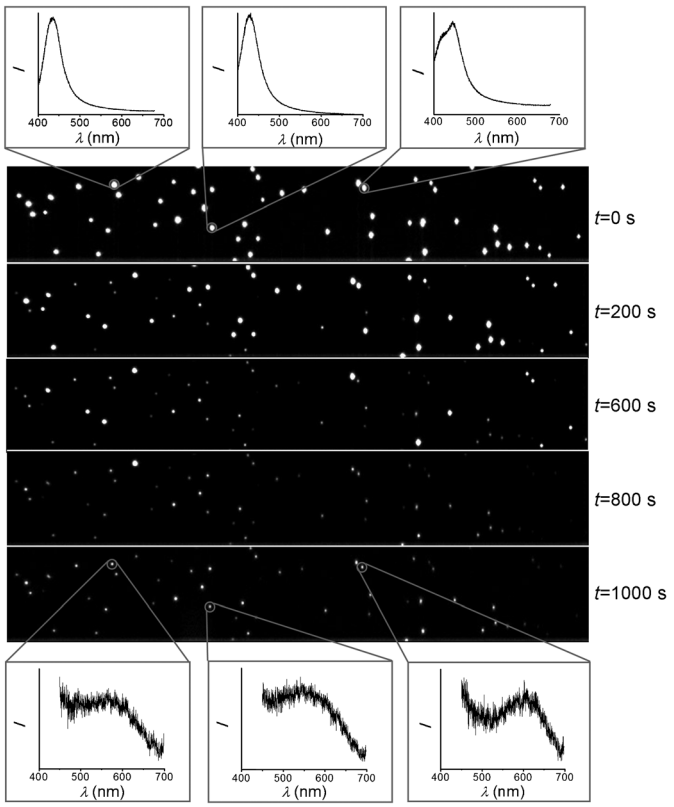

Figure 1. Single nanoparticles undergoing a galvanic exchange reaction. Dark-field scattering snapshots of a wide field of Ag nanoparticles show that as time progresses from $t=0$ s to $t=1000$ s, bright scatterers in the form of individual Ag nanoparticles (plasmon spectra are shown at the top for three representative nanoparticles) make a sharp conversion into dimly scattering Au/Ag nanocages (plasmon spectra are shown at the bottom for the same three nanoparticles). The full movie is included in the Supporting Information. The study was performed in a microfluidic flow cell with Ag nanoparticles immobilized on the flow-cell surface. $Au^{III}Cl_3$ (5 μM) was flowed at 1.5 mL h^{-1}. The time t indicated for each frame is relative to the instant in time when the $Au^{III}Cl_3$ solution entered the cell. The acquired movie and snapshots were corrected for stage drift. Spectra before the reaction were collected with a 10 s integration time, and those after the reaction with a 30 s integration time.

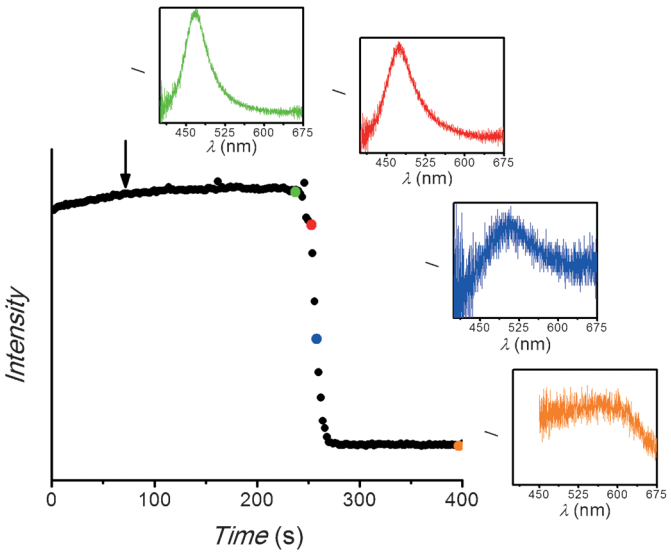

Figure 2. Trajectory for a single nanoparticle during a galvanic exchange reaction. The black trace shows the time trajectory of the scattering intensity of a single nanoparticle (integrated over approximately 400–680 nm) during galvanic exchange. Scattering spectra shown at four time points along the trajectory are indicative of a transformation from a Ag nanoparticle into a Au/Ag nanocage. The intensity trajectory shows that such a transformation is rapid for an individual nanoparticle. The reaction was performed with a 1.5 mL h^{-1} flow of the 3.5 μM $Au^{III}Cl_3$ solution. The Au^{3+} solution entered the cell at the instant indicated by the black arrow. Spectra were collected with a 2 s integration time and were corrected for dark counts and divided by the spectrum of the light source. The final spectrum (shown in orange) was collected with a 30 s integration time and corrected in the same way. Two more examples of representative single-particle trajectories from the same experiment can be found in Figure S1 of the Supporting Information.

(Figure 2). The initial and final plasmonic spectra are characteristic of Ag nanoparticles and Au/Ag nanocages, respectively.[26] The spectral red shift and decrease in scattering intensity always occurred simultaneously (Figure 2; see also Figure S1 in the Supporting Information), thus allowing us to infer reaction dynamics solely by tracking the scattering intensity of a wide field of several individual nanoparticles.

We analyzed several representative single-nanoparticle intensity trajectories (Figure 3, bottom colored traces). Following the start of the Au^{3+}-solution flow, each nanoparticle appears to "wait" a unique amount of time before making a transition from an Ag nanoparticle (high-scattering-intensity state) to the final Au/Ag nanocage structure (low-scattering-intensity state). Spectral movies confirmed that most of the spectral (and therefore structural) evolution of a nanostructure indeed took place during this intensity transition. The transitions of individual nanoparticles are

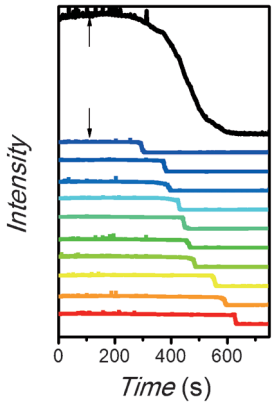

Figure 3. Galvanic exchange of single nanoparticles is much faster than conversion of the ensemble. The time trajectory of scattering intensity for an ensemble of nanoparticles (black trace) shows a gradual conversion of the ensemble. However, trajectories of several single nanoparticles (colored traces) show that the galvanic exchange of individual nanoparticles is rather rapid and occurs within a short time span. Individual nanoparticles undergo the exchange at different instants in time along the trajectory. In essence, the overall ensemble reaction is comprised of sharp transformation events of individual nanoparticles. A 6 μM $Au^{III}Cl_3$ solution flowing at 1.5 mL h^{-1} entered the microfluidic cell at the time indicated by the black arrow. The ensemble trajectory was obtained by summing intensities for all 129 nanoparticles.

seen to be rather rapid when compared to the much more gradual ensemble conversion (Figure 3, top black trace). In fact, the gradual ensemble-scale reaction progress is simply a collection of many sharp single-nanoparticle transitions occurring at various instants of time in the overall trajectory.

The dynamics represented by individual nanoparticle trajectories are characteristic of a system in which an initial critical event serves as a precursor to the transformation. The critical event has low probability; however, once it has occurred, the nanoparticle can make a rapid spontaneous transformation. The waiting time represents the time elapsed before a nanoparticle can stochastically undergo this critical event. As time progresses, the likelihood of such a critical event occurring increases, as reflected in the peak in the distribution of single-nanoparticle waiting times at an intermediate time (Figure 5a, left panel).

Critical intermediates in solid-state reactions typically involve the formation of a nucleation cluster or specific defects within the lattice.[1–3] To structurally identify the intermediate suggested by our single-nanoparticle trajectories, we performed high-angle annular dark-field scanning transmission electron microscopy (HAADF-STEM) imaging of the nanoparticles at various stages of galvanic exchange (Figure 4; see also Figure S5). The images confirmed that each nanostructure is initially a quasispherical Ag nanoparticle, which finally evolves into a nanocage composed of an Au/Ag alloy (see Figure S6 for elemental analysis).

Snapshots of individual nanostructures at an intermediate stage of galvanic exchange (Figure 4, middle row) were most revealing. At the intermediate stage, many of the nanoparticles exhibit surface voids. The formation of such a void may be a critical step in the galvanic-exchange transformation of a nanoparticle. It is widely believed that in the initial stages of galvanic replacement, Au deposition/alloying on the surface or the presence of a passivating oxide layer can block or passivate the Ag surface and limit the reaction rate by hindering solid-state out-diffusion of Ag.[26–29] However, higher-surface-energy regions, such as corners or grain boundaries, with higher oxidation potentials can exhibit favorable removal of Ag, and the resulting vacancies or pinhole defects can coalesce into a localized void.[30] Such a void can greatly enhance the out-diffusion of Ag^+ and thus enable the reaction to proceed at rates governed by diffusion in the liquid phase.[26–29] Newly formed Ag vacancies can coalesce with the void, thus allowing it to grow spontaneously until void growth culminates in a hollow cage structure.

Despite the identification of voids at the intermediate stage, we cannot rule out the possibility that initial Au clusters serve as critical nuclei for further deposition of Au. These initial nucleation clusters would be too small (a few atoms)[31] to be detected on the basis of spectral shifts. However, the templated nature of the galvanic exchange reaction and the cagelike structure of the final product strongly suggest that the critical phenomenon in the transformation involves the formation of a localized void in the Ag lattice rather than a Au nucleus. We observed in our TEM images that the extent of void formation varied greatly from one nanostructure to another, ranging from minimal (example shown in Figure 4, middle row, leftmost image) to high (Figure 4, middle row, rightmost image). This variation in the extent of void formation is consistent with the observed dispersion in the waiting times of single nanoparticles in the trajectories.

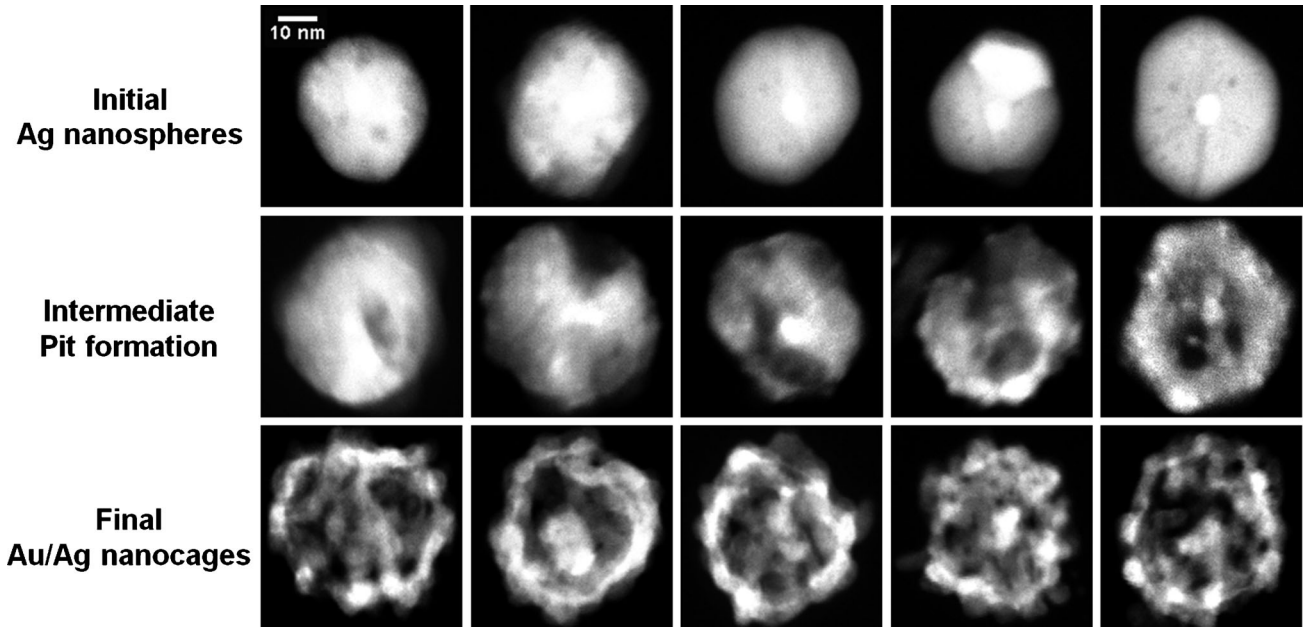

Figure 4. Electron microscopy images revealing structural aspects of the dynamics of galvanic exchange. Top: HAADF-STEM images of representative unreacted Ag nanospheres. Middle: Images of some representative partially exchanged nanoparticles. The images reveal voids formed within the nanoparticle. The degree of void formation varies from one nanoparticle to another. This variation in the degree of void formation is consistent with the observed dispersion in waiting times. Bottom: Images of the final nanostructures, which have the morphology of nanocages. The final composition is that of an Au/Ag alloy, as determined by energy dispersive spectroscopic analysis (see Figure S6). Samples for three different stages of exchange were obtained by titrating a solution of Ag nanospheres with increasing amounts of $Au^{III}Cl_3$ (see Figure S5).

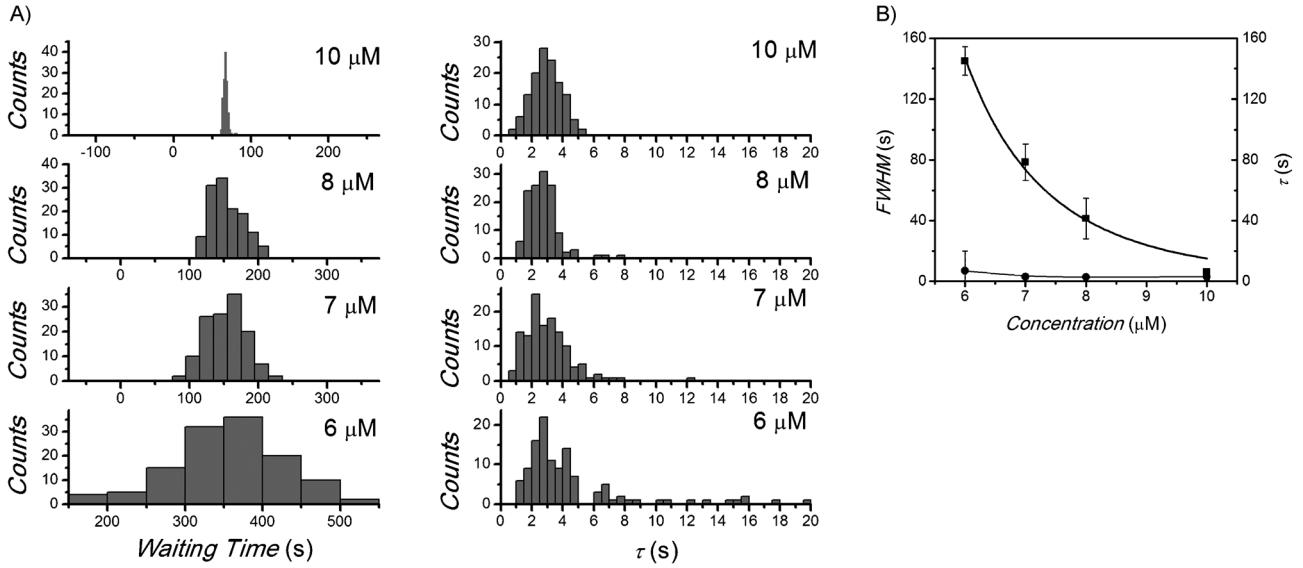

Figure 5. Single-nanoparticle dynamics versus ensemble behavior. A) Single-nanoparticle waiting times, shown on the left, follow a peaked distribution indicative of a process limited by a critical intermediate step. The dispersion of single-nanoparticle waiting times, indicated by the FWHM of this distribution, reflects the rate of the overall ensemble conversion. As the $Au^{III}Cl_3$ concentration is increased, the distribution narrows, which indicates an increase in the ensemble-conversion rate. On the right, the time constant τ for conversion is shown for several single nanoparticles in the form of a distribution. The time constant, on average, does not change when the $Au^{III}Cl_3$ concentration is increased, thus implying that it represents an intrinsic rate of mass-transport-limited exchange of a single nanoparticle. The ensemble rate is unaffected by this intrinsic single-nanoparticle rate, but is rather dependent on the dispersion of single-nanoparticle waiting times. Waiting times and time constants were derived from sigmoidal fitting of single-nanoparticle trajectories (see the Supporting Information for a more detailed description). Waiting times are relative to the instant at which the $Au^{III}Cl_3$ solution entered the flow cell. The assignment of the time of entry is somewhat approximate, as the region of interest is not located at the entrance of the flow cell. B) The FWHM of the waiting-time distribution (■, left axis) and the average time constant τ (●, right axis) are plotted as a function of the concentration. The FWHM values were obtained by Gaussian fitting of waiting-time distributions, with the error in the fit used as the magnitude of the error bar. For average time constants, the standard deviation was used as the error bar. The FWHM data were fit ($R^2 = 0.99$) to Equation (8) as shown by the curve drawn between the data points (■).

Although nanoparticle-to-nanoparticle variations in surface structure may contribute, to some extent, to the variation of single-nanoparticle waiting times, we found that the distribution of waiting times was primarily a result of the stochastic nature of the reaction. Measured waiting times of individual nanoparticles showed no correlation with their plasmonic scattering intensities or plasmon-resonance maxima: attributes that are sensitive to the size and shape of the nanoparticle (see Figure S8). Thus, the waiting time of a nanoparticle does not seem to be dictated by its size or shape, or even its spatial location in the flow cell (see Figure S4). Rather, the individual nanoparticle waiting times are stochastically distributed.

The considerable induction times observed indicate that the formation of a critical void is kinetically limiting.[32] Once a nanoparticle stochastically forms a spontaneously growing void, a relatively rapid transformation into the nanocage structure occurs, as seen in our optical-imaging trajectories. The formation of a single critical void within a nanoparticle may be sufficient to trigger complete galvanic exchange of the nanoparticle, as suggested by the absence of multiple steps in our single-nanoparticle trajectories. The relatively fast switching of individual nanoparticles as compared to the ensemble-conversion rate indicates that the rate of critical-void formation is significantly slower than the diffusion-limited exchange rate. The speed of the ensemble-scale reaction is therefore dictated by the rate of formation of critical voids. This rate depends on the concentration of incoming Au^{3+} ions, as manifested in two ways. First, the peak of the waiting-time distribution shifts to shorter times as the Au^{3+} concentration is increased (Figure 5a). Second, the dispersion in single-particle waiting times narrows with increasing concentration (Figure 5a). A narrower dispersion (i.e., smaller full width at half maximum, FWHM) is equivalent to a faster ensemble-scale conversion.

The intrinsic rate at which a single nanoparticle transforms, once the critical step has occurred, is essentially independent of the $Au^{III}Cl_3$ concentration (Figure 5a, right) and is most likely only mass-transport-limited. At high concentration (10 μm), when the rate of critical events is no longer limiting, the ensemble rate tends to the intrinsic single-particle exchange rate (Figure 5a, left). In other words, the waiting-time dispersion (FWHM) at 10 μm becomes extremely narrow, almost approaching the intrinsic single-particle switching time τ (Figure 5b). The waiting-time dispersion at high concentration would not be so narrow if nanoparticle-to-nanoparticle structural variations were a primary contributor to the waiting-time dispersion.

An important feature of the exchange reaction is the dramatic nonlinearity of its kinetics (Figure 5b; see also Figure S7), as expected for a process dictated by a critical phenomenon. A less than 2-fold decrease in the Au^{3+} concentration (from 10 to 6 μM) resulted in a 23-fold decrease in the rate of the reaction. Upon a further decrease in the

Au^{3+} concentration to 1 μM, absolutely no reaction was observed even after 1000 s (see Movie 4 in the Supporting Information). The total amount of Au^{3+} delivered to the flow cell over this time interval was the same as that delivered in the 5 μM experiment (see Movie 1 in the Supporting Information) by 234 s. The fact that several nanoparticles had exchanged in the 5 μM experiment by 234 s indicates that the amount of Au^{3+} delivered to the flow cell is not the factor limiting the progress of exchange in the 1 μM experiment. Rather, it is the significantly reduced rate of occurrence of critical events at this concentration that limits the reaction progress.

We ascribe this strong nonlinearity of the reaction kinetics to the dynamics involved in the formation of a critical void. The rate of critical-void formation is given by:

$$r \propto e^{-\Delta G_c/kT} \tag{1}$$

in which ΔG_c is the free-energy barrier for critical-void formation. For a spherical void comprised of n vacancies each of volume v, the net free energy of void formation is given by:

$$\Delta G^* = n g + 4\pi\left(\frac{3nv}{4\pi}\right)^{2/3}\gamma \tag{2}$$

in which γ is the surface tension between the Ag phase and the solution, which is assumed to fill the void; g is the free energy for the formation of a single Ag vacancy (V_{Ag}) according to the reaction:

$$AuCl_4^-(aq) + 3\,Ag(s) \rightarrow Ag(s) + 3\,V_{Ag} + 3\,AgCl + Cl^-(aq) \tag{3}$$

The surface-energy cost of creating a void [second term in Eq. (2)] increases with increasing surface area of the void as $n^{2/3}$, whereas the bulk-free-energy stabilization resulting from galvanic exchange [first term in Eq. (2)] increases with increasing volume of the void as n. Thus, when the void becomes a critical size n_c, the bulk-free-energy stabilization can offset the surface-energy cost. This situation is given by:

$$\frac{\partial \Delta G^*}{\partial n} = 0 \tag{4}$$

Solving Equation (4), we determine:

$$n_c = -\left(\frac{3v}{4\pi}\right)^2\left(\frac{8\pi\gamma}{3g}\right)^3 \tag{5}$$

Once the void size is greater than n_c, the total free energy decreases monotonically with size, thus allowing spontaneous progress of exchange through barrierless diffusion-limited growth of the void. Thus, $n = n_c$ is the point of maximum total free energy, which is essentially the free-energy barrier for the reaction, given as:

$$\Delta G_c = \frac{16\pi\gamma^3 v^2}{3g^2} \tag{6}$$

The rate of critical void formation becomes:

$$r \propto \exp\left(-\frac{16\pi\gamma^3 v^2}{3kTg^2}\right) \tag{7}$$

Each nanoparticle develops a critical void stochastically. The rate r is a measure of the likelihood per unit time of the formation of a critical void in an individual nanoparticle. Thus, the higher the rate of critical-void formation, the narrower is the dispersion of single-nanoparticle waiting times. This dispersion is inversely proportional to the critical-void-formation rate r:

$$\mathrm{FWHM} \propto \exp\left(-\frac{16\pi\gamma^3 v^2}{3kTg^2}\right) \tag{8}$$

The strong concentration dependence of this dispersion arises from:

$$g = \frac{1}{3}\left(g_0 - kT\cdot\ln\left[Au^{III}Cl_4^-\right]\right) \tag{9}$$

In Equation (9), g_0 is the standard free energy (225 kJ mol−1) for the galvanic exchange reaction indicated by Equation (3), and the factor 3 accounts for the fact that three Ag vacancies are created for every such reaction. This void-growth model, while simple, was able to simulate the strongly nonlinear trend of the reaction rate (see fit in Figure 5b) with a value of γ of 1.42 J m^{-2}, which is close to the range of previously reported values (0.7–1.3 J m^{-2}) for silver in aqueous media.[33] Note that the γ value estimated from the fit to our experimental data is an average over various types of atomic sites involved in the creation of a critical void. The somewhat higher value of γ estimated in this study, as compared to previously reported values, is possibly reflective of the contribution of higher-surface-energy features, such as kinks, corners, or edges, which are likely to be initial sites of void nucleation.

The critical size of the void was estimated to be approximately 20 atomic vacancies (sub-nanometer), beyond which the void grows spontaneously. It may be possible to capture the formation of such critical voids by means of an in situ TEM study of silver-nanoparticle exchange under the flow of a solution of Au^{3+} ions. However, liquid-cell TEM studies have found that, in solution, the electron beam causes the reduction of metal salts to form nanoparticles.[34] Thus, the perturbation caused by a 200 keV electron beam is too large to allow any reliable study of the reaction dynamics. The relatively minimal perturbation in the optical-microscopy approach used in this study is fundamentally advantageous in this regard.

In summary, the galvanic replacement of Ag within Ag nanoparticles with Au to form Au/Ag nanocages involves a critical step related to the formation of a void of approximately 20 atomic vacancies. Once a nanoparticle forms such a critical void, the transformation into a nanocage structure is spontaneous and rapid. As a result of these dynamics, the galvanic exchange reaction exhibits a strong nonlinearity: Over a relatively narrow window of concentrations, we observed evolution from no exchange (1 μm), to exchange governed by the rate of critical events (5–8 μm), and eventually to a mass-transport-limited regime (10 μm).

Importantly, we have demonstrated that the study of transformations with nanoscale resolution can reveal mechanistic information that is normally blurred by ensemble averaging. Although these studies were performed on a collection of spatially separated individual nanosized grains, the insight obtained should apply to a large polycrystalline material. It is likely that exchange kinetics similar to those observed in this study are at play in the galvanic corrosion of a macroscopic piece of Ag metal. The critical role of localized voids in allowing rapid corrosion explains the often observed surface roughening of the metal and the development of porosity. It should be possible to extend these studies to more industrially relevant systems (e.g. copper corrosion) for microscopic insight into the corrosion process.

Received: October 25, 2013
Revised: January 18, 2014
Published online: February 7, 2014

Keywords: galvanic reactions · nanoparticles · nanostructures · nucleation · single-particle spectroscopy

[1] R. W. Gurney, N. F. Mott, *Proc. R. Soc. London Ser. A* **1938**, *164*, 151 – 167.
[2] J. W. Cahn, *Acta Metall. Mater.* **1961**, *9*, 795 – 801.
[3] D. Gebauer, A. Vökel, H. Cölfen, *Science* **2008**, *322*, 1819 – 1822.
[4] W. Xu, J. S. Kong, Y. E. Yeh, P. Chen, *Nat. Mater.* **2008**, *7*, 992 – 996.
[5] C. Novo, A. M. Funston, P. Mulvaney, *Nat. Nanotechnol.* **2008**, *3*, 598 – 602.
[6] W. Xu, P. K. Jain, B. J. Beberwyck, A. P. Alivisatos, *J. Am. Chem. Soc.* **2012**, *134*, 3946 – 3949.
[7] P. Giersig, T. Ung, L. M. Liz-Marzán, P. Mulvaney, *Adv. Mater.* **1997**, *9*, 570 – 575.
[8] Y. Sun, B. T. Mayers, Y. Xia, *Nano Lett.* **2002**, *2*, 481 – 485.
[9] S. E. Skrabalak, L. Au, X. Li, Y. Xia, *Nat. Protoc.* **2007**, *2*, 2182 – 2190.
[10] G. L. Song, A. Atrens, *Adv. Eng. Mater.* **1999**, *1*, 11 – 33.
[11] D. W. DeBerry, *J. Electrochem. Soc.* **1985**, *132*, 1022 – 1026.
[12] A. Wittstock, V. Zielasek, J. Biener, C. M. Friend, M. Bäumer, *Science* **2010**, *327*, 319 – 322.
[13] Y. Sun, B. Mayers, Y. Xia, *Adv. Mater.* **2003**, *15*, 641 – 646.
[14] J. E. Macdonald, M. B. Sadan, L. Houben, I. Popov, U. Banin, *Nat. Mater.* **2010**, *9*, 810 – 815.
[15] F. Xiao, B. Yoo, K. H. Lee, N. V. Myung, *J. Am. Chem. Soc.* **2007**, *129*, 10068 – 10069.
[16] M. H. Oh, T. Yu, S.-H. Yu, B. Lim, K.-T. Ko, M.-G. Willinger, D.-H. Seo, B. H. Kim, M. G. Cho, J.-H. Park, K. Kang, Y.-E. Sung, N. Pinna, T. Hyeon, *Science* **2013**, *340*, 964 – 968.
[17] D. J. Campbell, F. Saeki, H. Cang, L. Au, J. Lee, X. Li, Y. Xia, *Nano Lett.* **2005**, *5*, 473 – 477.
[18] M. Mohl, A. Kumar, A. Leela, M. Reddy, A. Kukovecz, Z. Konya, I. Kiricsi, R. Vajtai, P. M. Ajayan, *J. Phys. Chem. C* **2010**, *114*, 389 – 393.
[19] Y. Sun, Y. Xia, *Anal. Chem.* **2002**, *74*, 5297 – 5305.
[20] J. Chen, J. M. McLellan, A. Siekkinen, Y. Xiong, Z. Li, Y. Xia, *J. Am. Chem. Soc.* **2006**, *128*, 14776 – 14777.
[21] C. Sönnichsen, T. Franzl, T. Wilk, G. von Plessen, J. Feldmann, O. Wilson, P. Mulvaney, *Phys. Rev. Lett.* **2002**, *88*, 077402.
[22] A. Tcherniak, S. Dominguez-Medina, W. S. Chang, P. Swanglap, L. S. Slaughter, C. F. Landes, S. Link, *J. Phys. Chem. C* **2011**, *115*, 15938 – 15949.
[23] L. J. Sherry, R. Jin, C. A. Mirkin, G. C. Schatz, R. P. Van Duyne, *Nano Lett.* **2006**, *6*, 2060 – 2065.
[24] S. Sheikholeslami, Y. Jun, P. K. Jain, A. P. Alivisatos, *Nano Lett.* **2010**, *10*, 2655 – 2660.
[25] A. E. Schlather, N. Large, A. S. Urban, P. Norlander, N. J. Halas, *Nano Lett.* **2013**, *13*, 3281 – 3286.
[26] M. H. Kim, X. Lu, B. Wiley, E. P. Lee, Y. Xia, *J. Phys. Chem. C* **2008**, *112*, 7872 – 7876.
[27] E. González, J. Arbiol, V. F. Puntes, *Science* **2011**, *334*, 1377 – 1380.
[28] Y. Sun, Y. Xia, *Nano Lett.* **2003**, *3*, 1569 – 1572.
[29] Y. Sun, Y. Xia, *J. Am. Chem. Soc.* **2004**, *126*, 3892 – 3901.
[30] "Mechanisms of Pitting Corrosion": H.-H. Strehblow in *Corrosion Mechanisms in Theory and Practice*, 3rd ed. (Ed.: P. Marcus), CRC, Boca Ranton, **2012**.
[31] E. Budevski, G. Staikov, W. J. Lorenz, *Electrochim. Acta* **2000**, *45*, 2559 – 2574.
[32] C. Punckt, M. Bölscher, H. H. Rotermund, A. S. Mikhailov, L. Organ, N. Budiansky, J. R. Scully, J. L. Hudson, *Science* **2004**, *305*, 1133 – 1136.
[33] S. F. Chernov, Y. V. Fedorov, V. N. Zakharov, *J. Phys. Chem. Solids* **1993**, *54*, 963 – 966.
[34] J. M. Yuk, J. Park, P. Ercius, K. Kim, D. J. Hellebusch, M. F. Crommie, J. Y. Lee, A. Zettl, A. P. Alivisatos, *Science* **2012**, *336*, 61 – 64.

